

Cell information processing via frequency encoding and excitability

Alan Givré & Silvina Ponce Dawson

UBA, FCEN, Departamento de Física & CONICET-UBA, IFIBA,
Ciudad Universitaria Pab. I, (1428) Buenos Aires, Argentina

E-mail: silvina@df.uba.ar

April 2024

Abstract. Cells continuously interact with their environment mediating their responses through *signaling cascades*. Very often, external stimuli induce pulsatile behaviors in intermediaries of the cascade of increasing frequency with the stimulus strength. This is characteristic of intracellular Ca^{2+} signals involving Ca^{2+} release through Inositol Trisphosphate Receptors (IP_3Rs). The mean frequency of IP_3R -mediated Ca^{2+} pulses has been observed to scale exponentially with the stimulus strength in many cell types. In this paper we use a simple ODE model of the intracellular Ca^{2+} dynamics for parameters for which there is one excitable fixed point. Including fluctuations through an additive noise term, we derive the mean escape rate from the stationary state and, thus, the mean interpulse time, as a function of the fraction, β , of readily openable IP_3Rs . Using an IP_3R kinetic model, experimental observations of spatially resolved Ca^{2+} signals and previous estimates of the IP_3 produced upon stimulation we quantify the fluctuations and relate β to $[\text{IP}_3]$ and the stimulus strength. In this way we determine that the mean interpulse time can be approximated by an exponential function of the latter for ranges such that the covered mean time intervals are similar or larger than those observed experimentally. The study thus provides an easily interpretable explanation, applicable to other pulsatile signaling intermediaries, of the observed exponential dependence between frequency and stimulus, a key feature that makes frequency encoding qualitatively different from other ways commonly used by cells to “read” their environment.

1. Introduction

Cells continuously interact with their surroundings, not only to exchange nutrients and energy, but also to detect environmental changes and act accordingly [1]. Very frequently changes in the environment are endowed in concentration changes of substances that can bind to plasma membrane receptors. This, in turn, induces changes in the concentration and/or activation level of various intracellular components in what is known as a *signaling cascade*. Cells use different strategies to go from the external stimulus to the end response [2, 3, 4]. Sometimes, increasing intensities of the external stimulus are “encoded” in increasing concentrations of the internal *messengers*

(amplitude codification) [5]. On other occasions, stimuli induce a pulsatile behavior in some of the intermediaries in which the frequency increases with the stimulus strength (frequency encoding) [6, 7]. This last behavior has been observed in intracellular Ca^{2+} signals [8, 9] that involve Ca^{2+} release from the endoplasmic reticulum (ER) through Inositol Trisphosphate Receptors (IP_3Rs) [10].

Ca^{2+} is ubiquitous as intracellular messenger. It is involved in the control of many cellular functions including both fertilization and cell death [11]. On many occasions, the selective control of specific targets depends on the spatio-temporal of the cytosolic Ca^{2+} concentration. Ca^{2+} release from the ER through IP_3Rs give cells the tools to produce different spatio-temporal patterns. On one hand, IP_3Rs need to bind IP_3 and Ca^{2+} to become open. Therefore, the opening of one such channel can lead to the opening of many others due to *Calcium Induced Calcium Release* [12]. IP_3Rs , in turn, are usually organized in clusters containing $\sim 10-20$ channels. Furthermore, high Ca^{2+} concentrations inhibit IP_3Rs . Thus, the signals can range from *blips* and *puffs* involving Ca^{2+} release from one channel or cluster, to waves that propagate throughout the cell depending on the level of IP_3 [13, 14, 15] and the interplay between Ca^{2+} activation and inhibition. Under physiological conditions, IP_3 is made via the hydrolysis of precursors that are on the plasma membrane by the enzyme Phospholipase C (PLC) which is activated as a result of the binding of external effectors to specific plasma membrane receptors. In many different cell types, constant stimulation with extracellular ligands can yield sequences of these waves that, when the interior of the cell is not resolved, are visualized with fluorescence microscopy techniques as sequences of Ca^{2+} spikes [8, 9]. Usually each Ca^{2+} spike is preceded by localized signals which start to occur more frequently until they yield the global release event [16]. This is typical of spatially extended excitable systems in which random local (Ca^{2+} release) events are amplified through space eventually triggering an “extreme” one (a Ca^{2+} spike) [17, 18]. We hereby recall the defining characteristics of excitable systems: the existence of a stable stationary state, a threshold which, if surpassed by perturbations, a long excursion in phase space occurs before the system returns to the stationary solution and a refractory period before a new spike can be elicited by perturbations [19].

A systematic study of intracellular Ca^{2+} pulses evoked by constant concentrations of extracellular ligands showed, in many cell types, that the interspike time interval could be approximated by the sum of a fixed term, T_{min} , accounting for spike duration and refractoriness, and a stochastic term, T_{stoch} , of average, $T_{av} \equiv \langle T_{stoch} \rangle$ which depended exponentially on the extracellular concentration [9]. This dependence which we have already used to study information transmission via frequency encoding [20, 21], resembles that of thermally activated barrier crossing [22], where the crossing rate is an exponential function of the activation energy threshold. A similar behavior occurs for the average escape time in noise-driven excitable systems [23] in which the external perturbation either increases the noise level or reduces the excitability threshold [24, 25, 26]. The dynamics of intracellular Ca^{2+} has been associated with excitability [27, 28], various models of this dynamics are excitable [29, 30, 31, 32] and

have even been used to study information transmission via frequency encoding although under the assumption of a linear relation between frequency and stimulus strength [30]. In this paper we study whether the experimentally observed exponential dependence of the average time interval between subsequent Ca^{2+} spikes can be derived from an excitable model of intracellular Ca^{2+} dynamics. Using the simple model developed by Dupont and Goldbeter [33] we derive the mean escape rate from the stationary state. Combining this result with the DeYoung-Keizer kinetic model of IP_3 Rs [34] and experimental observations of Ca^{2+} signals elicited in *X. Laevis* oocytes [16], we determine how the escape rate depends on the IP_3 concentration and, consequently, on the external stimulus strength under the assumption that it is proportional to $[\text{IP}_3]$. This derivation provides a theoretical framework to support our recent study which shows that frequency and amplitude encodings equip cells with qualitatively different tools to sense their environment [21].

2. The model

In this work we use the very simple one-pool model of intracellular Ca^{2+} dynamics introduced by Dupont and Goldbeter [33]. The equations defining this model are:

$$\begin{aligned} \dot{C} = & v_0 + v_1\beta - v_{M2}\frac{C^n}{K_2^n + C^n} + \beta v_{M3}\frac{C^p}{K_A^p + C^p}\frac{Y^m}{K_R^m + Y^m} \\ & + k_f Y - kC, \end{aligned} \quad (1)$$

$$\dot{Y} = v_{M2}\frac{C^n}{K_2^n + C^n} - \beta v_{M3}\frac{C^p}{K_A^p + C^p}\frac{Y^m}{K_R^m + Y^m} - k_f Y, \quad (2)$$

where C is the free Ca^{2+} concentration in the cytosol and Y can be assumed to be proportional to the free $[\text{Ca}^{2+}]$ in the lumen of the ER with the constant of proportionality taking into consideration the ratio of the luminal to the cytosolic volumes and of the Ca^{2+} buffering capacities in both pools [35]; v_0 represents the Ca^{2+} influx from the extracellular medium; the two terms proportional to β represent the IP_3 -dependent release of Ca^{2+} from the ER with $0 \leq \beta \leq 1$, the fraction of IP_3 -bound IP_3 Rs; the term proportional to v_{M2} represents Ca^{2+} pumping back into the ER, the term $k_f Y$ a Ca^{2+} leak from the ER and the last term in Eq. (1) is the removal of free cytosolic Ca^{2+} by various means. To facilitate the computations, as done in [36], we introduce the variable $Z \equiv C + Y$ and rewrite Eqs. (1)–(2) as:

$$\begin{aligned} \dot{C} = & v_0 + v_1\beta - v_{M2}\frac{C^n}{K_2^n + C^n} + \beta v_{M3}\frac{C^p}{K_A^p + C^p}\frac{(Z - C)^m}{K_R^m + (Z - C)^m} \\ & + k_f(Z - C) - kC, \end{aligned} \quad (3)$$

$$\dot{Z} = v_0 + v_1\beta - kC. \quad (4)$$

In this paper we use the parameter values introduced in [33] as listed in Table 1. The only parameter that we change with respect to those of [33] is β , since the value $\beta = 0.4$ used in that paper yields oscillations while we are after an excitable behavior. As explained in what follows, in the model, increments in stimulus strength are represented

Parameter	Value
v_0	$3.4\mu Mmin^{-1}$
v_1	$3.4\mu Mmin^{-1}$
v_{M2}	$50\mu Mmin^{-1}$
v_{M3}	$650\mu Mmin^{-1}$
K_A	$0.9\mu M$
K_2	$1\mu M$
K_R	$2\mu M$
k_f	$1min^{-1}$
k	$10min^{-1}$
p	4
m	2
n	2

Table 1. Model parameters that we use in this paper, as introduced in [33].

by increments in β . The aim of our calculations here is to determine the dependence with β of the probability per unit time that a spike is elicited for values of β for which the dynamical system is excitable. Relating β with $[IP_3]$ and, eventually, with the external stimulus strength, I_{ext} , we expect to determine the conditions under which this probability is an exponential function of I_{ext} . Under these conditions, the occurrence of a spike will be a Poisson process with an average inter-spike period that decreases exponentially with the stimulus strength.

3. Analysis of the model

3.1. External stimuli and the parameter β .

Eqs. (3)–(4) model the dynamics of intracellular Ca^{2+} when Ca^{2+} release through IP_3Rs is involved. As already mentioned, IP_3Rs need to bind (cytosolic) Ca^{2+} and IP_3 to become open and, normally, IP_3 is produced upon stimulation with external effectors such as hormones or neurotransmitters. The model does not include an explicit description of IP_3 production. The effect of the external stimulus is implicitly included *via* the parameter β which represents the fraction of IP_3Rs with IP_3 bound that are ready to become open upon Ca^{2+} binding. Increments in stimulus strength are thus represented by increments in β . Dupont and Goldbeter analyzed the bifurcation diagram of the model for the parameters in Table 1 and $\beta \in (0, 1)$ [33]. They determined that there is a stable fixed point for $\beta \lesssim 0.24$ and for $\beta \gtrsim 0.8$ and a stable limit cycle for β values in between. In what follows we analyze the values of β for which the stable fixed point is excitable.

3.2. Equilibrium solutions and nullclines.

We show in Fig. 1 the nullclines of the model for three values of β . We observe that for all $0 \leq \beta \leq 1$ there is only one fixed point, (C_{eq}, Z_{eq}) , which satisfies:

$$C_{eq} = \frac{v_0 + v_1\beta}{k}. \quad (5)$$

Thus, C_{eq} increases with β . On the other hand, for all cases it is $\dot{Z} > 0$ ($\dot{Z} < 0$) to the left (right) of the nullcline depicted with dashed lines while $\dot{C} > 0$ ($\dot{C} < 0$) in the region above (below) the nullcline depicted with solid lines. This is equivalent to the nullcline structure of a prototypical example of excitability, the FitzHugh-Nagumo (FHN) model, if we identify $-Z$ and C of Eqs. (3)–(4) with the slow and fast variables of the FHN model, respectively [19]. Thus, as the nullclines cross to the left of the value, C , at which the \dot{C} nullcline has its local maximum, the fixed point is excitable as illustrated in what follows. In fact, for the case of Fig. 1 (a), which corresponds to $\beta = 0.09$, the only fixed point is excitable: initial conditions that start on one or the other side of the “middle branch” of the \dot{C} nullcline either give rise to a relatively long excursion in phase space or decay monotonically to the fixed point. This is illustrated in Fig. 2 (a) where we have plotted the time evolution of C for $\beta = 0.09$ and two such initial conditions. As β is increased, C_{eq} gets closer to the value at which the \dot{C} nullcline has its local maximum. The equilibrium solution continues to be excitable as long as C_{eq} is bounded away from this local maximum, *e.g.*, for $\beta = 0.15$ for which we show the nullclines and two trajectories in Figs. 1 (b) and 2 (b), respectively. It can be observed in Fig. 2 (b) that the excursion in phase space is larger than in 2 (a), consistently with the structure of the nullclines. At $\beta \approx 0.183$ the fixed point becomes a stable focus and then loses stability at $\beta \approx 0.237$ through a Hopf bifurcation. For $0.237 \lesssim \beta \lesssim 0.775$ the stable (asymptotic) solution is a limit cycle, as illustrated in Fig. 2 (c) which corresponds to $\beta = 0.3$ for which the nullclines are plotted in Fig. 1 (c). As β gets closer from below to $\beta = 0.775$, the oscillations become more sinusoidal and of smaller amplitude until a new Hopf bifurcation, at $\beta \approx 0.775$, makes the fixed point stable again for larger values of β . For $\beta \gtrsim 0.8$, perturbations to the fixed point do not yield solutions in which C increases significantly with respect to the stationary solution value. Thus, this region does not correspond to an excitable regime in which Ca^{2+} pulses can be elicited. Thus, for our purposes, from now on we will restrict the analysis to $\beta \leq 0.22$ to guarantee the excitability of the system.

The simple model provides reasonable values of C_{eq} and Y_{eq} for the range of parameters for which the only stable solution is excitable. Namely, in most cell types, the free cytosolic Ca^{2+} concentration is very small at basal levels ($\sim 50 - 100 \text{ nM}$ [37]), consistent with the values depicted in Fig. 3 (which satisfy $C_{eq} \sim 0.4 \mu\text{M}$ throughout the figure). In *X. Laevis* oocytes, the free Ca^{2+} concentration in the lumen of the ER was estimated to be $\sim 200 \mu\text{M}$, the ratio of the luminal to the cytosolic volume as 0.7 and that of the fraction of free Ca^{2+} in the cytosol and in the ER as 0.00125 [35]. In a mechanistic interpretation of Eqs. (1)–(2), Y could be identified with the product of

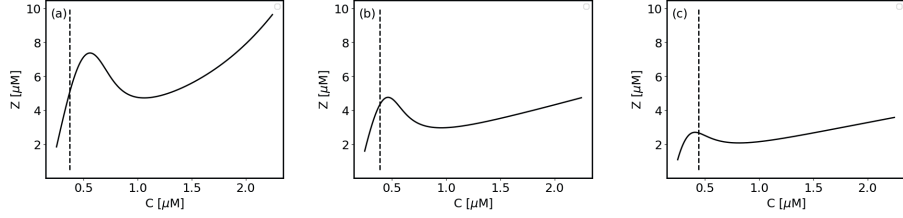


Figure 1. Nullclines of the model given by Eqs. (3)–(4) for the parameter values of Table 1 and $\beta = 0.09$ (a), $\beta = 0.15$ (b) and $\beta = 0.3$ (c).

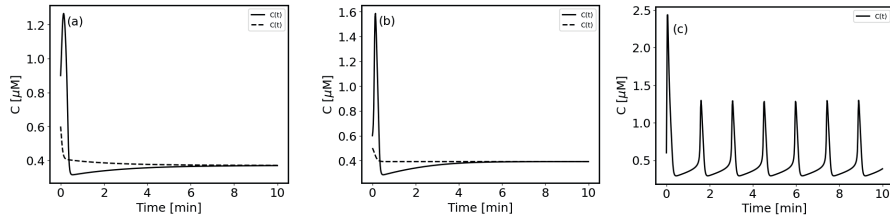


Figure 2. Time course of C derived by solving Eqs. (3)–(4) for the same parameter values as in Fig. 1. In (a) and (b) we show the time evolution for two initial conditions to illustrate that the only fixed point of the system is stable but excitable. In (c) there is a stable limit cycle.

these two ratios (~ 0.009) times the free luminal Ca^{2+} concentration. Thus, equilibrium values, $Y_{eq} \sim 3.5 - 4\mu\text{M}$, as those that can be derived from Fig. 3, are consistent with the estimates of [35].

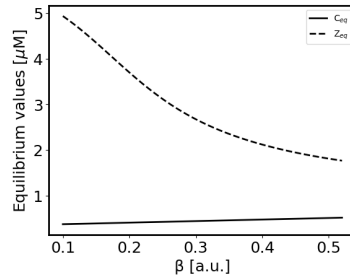


Figure 3. Equilibrium concentrations, C_{eq} and Z_{eq} , for values of β for which the only equilibrium solution is excitable. The corresponding Ca^{2+} concentration in the lumen of the ER can be derived from $Y_{eq} = Z_{eq} - C_{eq}$.

3.3. Slow and fast variables

The equilibrium values, C_{eq} and Z_{eq} , displayed in Fig. 3 differ by about an order of magnitude. On the other hand, during the (relatively short) pulses elicited in C such as the one illustrated in Fig. 2 (b), C increases by a factor smaller than 4. As it is standard

for the analysis of reactions with enzymes in the quasi-stationary approximation [38], we introduce dimensionless concentrations, $\bar{C} = C/C_{eq}$ and $\bar{Z} = Z/Z_{eq}$ and time, $\tau = tv_0/C_{max}$, to rewrite Eqs. (3)–(4) as:

$$\begin{aligned} \frac{d\bar{C}}{d\tau} = & 1 + \frac{v_1}{v_0}\beta - \frac{v_{M2}}{v_0} \frac{\bar{C}^n}{K_2^n + \bar{C}^n} + \beta \frac{v_{M3}}{v_0} \frac{\bar{C}^p}{K_A^p + \bar{C}^p} \frac{(\bar{Z}/\epsilon - \bar{C})^m}{K_R^m + (\bar{Z}/\epsilon - \bar{C})^m} \\ & + \frac{k_f}{v_0}(\bar{Z}/\epsilon - \bar{C}) - \frac{kC_{max}\bar{C}}{v_0}, \end{aligned} \quad (6)$$

$$\frac{d\bar{Z}}{d\tau} = \epsilon \left(1 + \frac{v_1}{v_0}\beta - \frac{kC_{max}\bar{C}}{v_0} \right), \quad (7)$$

where $\epsilon \equiv C_{eq}/Z_{eq} \ll 1$. It is clear from Eqs. (6-7) that \bar{Z} (and, thus, Z) is the slow variable. This time scale separation is further reinforced by the choice of parameter values of Table 1 which are such that v_{M3} , that only affects the dynamics of C , is a much faster rate than all the others.

4. Spike occurrence and interspike time average.

We study the probability of spike occurrence per unit time restricting the analysis to the dynamics on the fast manifold. Namely, we fix $0.1 \leq \beta \leq 0.22$, $Z = Z_{eq}(\beta)$ and work with the equation:

$$\begin{aligned} \dot{C} = & v_0 + v_1\beta - v_{M2} \frac{C^n}{K_2^n + C^n} + \beta v_{M3} \frac{C^p}{K_A^p + C^p} \frac{(Z_{eq}(\beta) - C)^m}{K_R^m + (Z_{eq}(\beta) - C)^m} \\ & + k_f(Z_{eq}(\beta) - C) - kC \equiv -\frac{dV_\beta}{dC}, \end{aligned} \quad (8)$$

where we have introduced the definition of the potential, $V_\beta(C)$. The rate of spike occurrence derived from the analysis of Eq. (8) will give the stochastic component of the interspike time. The total interspike time will then be the sum of this stochastic component, the spike duration and the recovery time (which is not accounted for by Eq. (8)).

As already explained, v_0 and $k_f Y = k_f(Z_{eq} - C)$ in Eq. (8) represent an influx of Ca^{2+} in the cytosol from the extracellular medium and the ER, respectively, that is independent of cytosolic Ca^{2+} and IP_3 . There is an additional IP_3 -dependent term, $v_1\beta$, which was included to account for the observation that the mean cytosolic $[\text{Ca}^{2+}]$ increases with the level of stimulation [33]. All these processes are affected by noise, since they are the net result of localized events of Ca^{2+} entry. Furthermore, as explained later in more detail, Ca^{2+} spikes correspond to waves that propagate throughout the cell which are preceded by spatially localized Ca^{2+} release events from the ER (puffs). As discussed in Sec. 5, puffs can be accounted for as a noise term added to the dynamic equation of the spatially averaged Ca^{2+} concentration, C . In fact, in that Section we use puffs data to estimate noise amplitude. The IP_3 produced as a consequence of the external stimulus can also fluctuate so that β is subject to random fluctuations as well. Assuming that, for each level of external stimulation, I_{ext} , fluctuations in β , $\delta\beta(I_{ext})$,

satisfy $\delta\beta(I_{ext}) \ll \langle\beta\rangle(I_{ext})$, we can embrace all the noisy part of these processes in a single additive term and rewrite Eq. (8) as:

$$\dot{C} = -\frac{dV_\beta}{dC} + \zeta, \quad (9)$$

with $\beta \cong \langle\beta\rangle(I_{ext})$. For simplicity, we further approximate ζ as a Gaussian white noise term with $\langle\zeta(t)\zeta(t')\rangle = 2D\delta(t-t')$ where D can, in principle, vary with β . We discuss later to what extent it is reasonable to assume that $\delta\beta(I_{ext}) \ll \langle\beta\rangle(I_{ext})$ and the implications of the β dependence of the coefficient, D .

We show in Figs. 4 (a) and (b) a plot of $V_\beta(C)$ for the same values of β as in Figs. 1 (a) and (b). We observe that, in both cases, there are two local minima, C_1 and C_2 , that correspond to stable fixed points of Eq. (9) and between them a saddle point, C_S , that determines the separatrix between basins of attraction (on the fast manifold). One of the stable fixed points of Eq.(8) is $C_1 = C_{eq}(\beta)$, *i.e.*, corresponds to the stationary (excitable) solution of the full (two-dimensional) model (Eqs. (3)-(4)). The difference, $\Delta V_\beta \equiv V_\beta(C_S) - V_\beta(C_1)$, is the height of the barrier that needs to be surpassed for the system (restricted to the fast manifold) to go from C_1 to C_2 . In the actual model, given by Eqs. (3)-(4), if $\beta \lesssim 0.22$, surpassing this barrier implies that the system undergoes a long excursion in phase space, therefore, a spike is elicited. This height decreases with β as shown in Fig. 4 (c) a plot of ΔV_β .

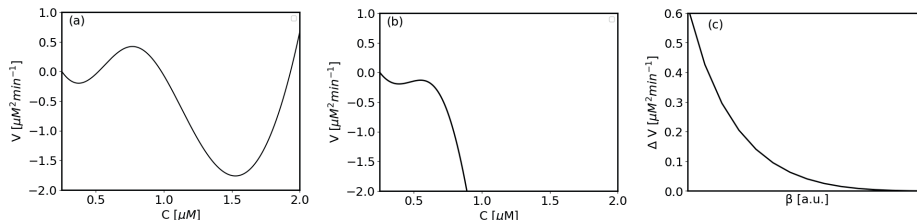


Figure 4. The potential, V_β , that determines the dynamics on the fast manifold (Eq. (9)) for $\beta = 0.09$ (a) and $\beta = 0.15$ (b) and the height of the barrier, $\Delta V_\beta \equiv V_\beta(C_S) - V_\beta(C_1)$, as a function of β , where C_S corresponds to the local maximum of V_β and C_1 to the local minimum to the left of C_S (which is the value at the equilibrium solution of Eqs. (3)–(4)).

For a bistable V_β (as in Figs. 4 (a)-(b)) Eq. (9) corresponds to the paradigmatic equation analyzed by Kramers [22] who obtained that the time it takes for the system to leave the vicinity of the local minimum, C_1 (which corresponds to the excitable fixed point of Eqs. (3)–(4)) is exponentially distributed with escape rate, r_β , that, in the low-noise limit ($D \ll \Delta V_\beta$), can be approximated by:

$$r_\beta = \frac{(V_\beta''(C_1)|V_\beta''(C_S))^{1/2}}{2\pi} \exp(-\Delta V_\beta/D), \quad (10)$$

with $V_\beta'' = d^2V_\beta/dC^2$. Thus, the mean interspike time, $\langle T_{IS} \rangle$, would be:

$$\langle T_{IS} \rangle = T_{min} + \frac{2\pi}{(V_\beta''(C_1)|V_\beta''(C_S))^{1/2}} \exp(\Delta V_\beta/D), \quad (11)$$

with T_{min} the sum of the spike duration and the recovery time. $\langle T_{IS} \rangle$ depends exponentially on ΔV_β which is a decreasing function of β (see Fig. 4 (c)) and, thus, of the external stimulus strength, I_{ext} . In the following Section we combine a variety of previously published results to derive the dependence of $\langle T_{IS} \rangle$ with I_{ext} within the framework of the very simple model considered in this paper.

5. Interspike time average and external stimulus strength

In order to determine the dependence of ΔV_β with I_{ext} we need to estimate the noise level (which enters through D in Eq. (11)) and the relation between β and I_{ext} . For the latter we need to relate β to the IP_3 concentration. We recall here that β is the fraction of IP_3 Rs with IP_3 bound that are ready to become open upon Ca^{2+} binding. To estimate β we use the DeYoung-Keizer model [34] which considers the tetrameric structure of the channel and assumes that three of the monomers need to have IP_3 bound and the Ca^{2+} inhibitory site free to eventually become open (upon Ca^{2+} binding to the activating site in the three monomers with IP_3 bound). The dissociation constant of the IP_3 -binding unbinding reaction depends on whether Ca^{2+} is bound or not to the inhibitory site. Assuming that immediately before the spike is elicited $[Ca^{2+}]$ is approximately equal to its low basal value so that the Ca^{2+} inhibitory site of the receptor is very likely free of Ca^{2+} , we use the dissociation constant that corresponds to the Ca^{2+} free situation, $K_{IP} = 0.13\mu M$, and relate β and $[IP_3]$ as:

$$\beta = \left(\frac{[IP_3]}{[IP_3] + K_{IP}} \right)^3. \quad (12)$$

We show in Fig. 5 (a) a plot of $[IP_3]$ vs β derived from Eq. (12) with $K_{IP} = 0.13\mu M$. We observe that the relation between $[IP_3]$ and β is approximately linear over the range of β values for which the dynamics of the simple model (Eqs. (3)–(4)) is excitable with slope $d\beta/d[IP_3] \sim 1.4$. On the other hand, the range of $[IP_3]$ values corresponds to having ~ 100 molecules/ μm^3 . Cell sizes vary over various orders of magnitude. The volume of the cells used in the experiments in which the exponential scaling between external stimulus strength and interpulse times was observed (hepatocytes and HEK293 cells [9]) are between 10^3 and $3 \cdot 10^4 \mu m^3$. Thus, according to our estimates, in the excitable regime, the number of IP_3 molecules in these cells is between 10^5 and $3 \cdot 10^6$. Using Poisson statistics to estimate the ratio between the fluctuations and the mean of this number we conclude that $\delta\beta/\langle\beta\rangle$, which is equal to this ratio, ranges between $4 \cdot 10^{-4}$ and $3 \cdot 10^{-3}$. Thus, according to these estimates, it is reasonable to assume that $\delta\beta \ll \langle\beta\rangle$ and that the effect of noise on the model can be approximated by an additive term in Eq. (3).

To estimate the noise level at fixed β , we use the experiments of [16] in which the authors analyzed the frequency and amplitude of the Ca^{2+} puffs (spatially localized Ca^{2+} signals due to the release through one cluster of IP_3 Rs) that occurred before a global Ca^{2+} wave (a spike) in *Xenopus Laevis* oocytes in the presence of different constant values of intracellular $[IP_3]$. For our calculation we assume that the Ca^{2+} puffs are the main random release events that enter in the noise term, ζ . In the

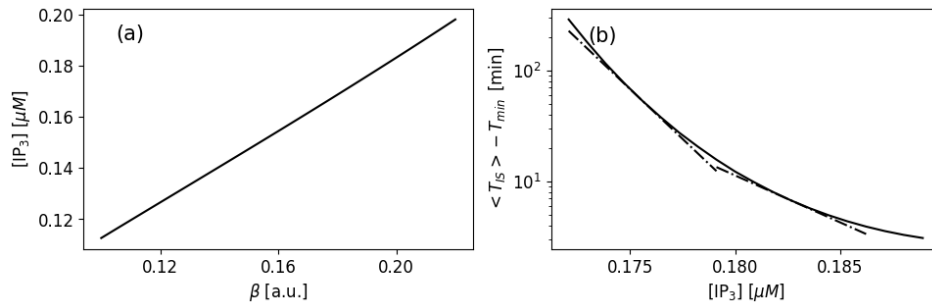


Figure 5. (a) $[IP_3]$ as a function of the IP_3 Rs saturation level, β , given by Eq. (12) with $K_{IP} = 0.13\mu M$. (b) Mean stochastic part of the interspike time, $\langle T_{IS} \rangle - T_{min}$ as a function of $[IP_3]$ obtained by combining Eqs. (12) and (11) with $D = 0.0015\mu M^2/min$ and $K_{IP} = 0.13\mu M$. Two straight lines tangent to the plotted curve at $[IP_3] \approx 0.176\mu M$ and at $[IP_3] \approx 0.183\mu M$ are also shown.

experiments [16], the Ca^{2+} signals were observed using the Ca^{2+} dye, Fluo4, and confocal microscopy scanning a $65\mu m \times 65\mu m$ region. The fluorescence associated to each puff was collected from a $8\mu m \times 8\mu m$ region. For the analysis, the authors separated the observations depending on the typical mean interspike time, which, as expected, decreased as the amount of released IP_3 increased, and could analyze the puffs for intermediate (between 25 and 50s) and high (mostly, between 50s and 70s) values of $\langle T_{IS} \rangle$. In both situations they observed that the amplitude of the puffs remained approximately the same. They measured the amplitude in terms of the relative increase of the fluorescence with respect to its basal level, $\Delta F/F_0$, obtaining $\Delta F/F_0 \sim 1$ in most cases. This implies that the local increase in $[Ca^{2+}]$ due to a single puff was of the order of the basal Ca^{2+} concentration ($0.4\mu M$ in our simple model, see Fig. 3). Now, in our model (Eqs. (3)–(4)), C corresponds to the concentration averaged over all the cell. Considering the $8\mu m \times 8\mu m$ region that was used to monitor puffs in [16], we assume that the increase in the cell-averaged concentration due to a single puff is $\sim (8/16)^2 0.4\mu M \approx 0.006\mu M$. Then, in the case of intermediate interspike times (mean values in 25 – 50 s), puffs start to occur approximately after 25% of the interspike time has elapsed (*i.e.*, during 19– 38 s) and the number of puffs is ~ 1000 so that the number of puffs per unit time is $\sim (26 – 53)/s$. Therefore, on average, the noise term amplitude is $\zeta \sim (26 – 53)0.006\mu M/s = (0.16 – 0.32)\mu M/s$. For the Kramers calculation we assumed that $\langle \zeta(t)\zeta(t') \rangle = 2D\delta(t – t')$. Puffs are not instantaneous, so that we will approximate $\delta(t – t')$ by the puff duration. Here we have two options, in one case, to take into account the duration of the release of Ca^{2+} or of the local Ca^{2+} elevation (estimated, respectively, as 20 and 150ms in [39]). Using the latter, we then estimate $D \sim (0.16^2 – 0.32^2)\mu M^2/s^2 \times 0.15s/2 = (0.002 – 0.007)\mu M^2/s = (0.13 – 0.46)\mu M^2/min$. Now, in the experiments with large mean interspike time (most of them between 50s and 70s), the number of puffs between spikes is about 120 and although the majority occurs after 25% of the interspike time has elapsed (*i.e.*, during 38 – 45s), there is a non-negligible fraction that occurs before. Thus, the number of puffs per unit

time is $\sim (2 - 3)/s$, much smaller than for intermediate values of $\langle T_{IS} \rangle$, while the amplitude remains approximately equal. Repeating the calculation for this smaller puff frequency we obtain $\zeta \sim (2 - 3)0.006\mu M/s = (0.012 - 0.018)\mu M/s$ which yields $D \sim (1.1 - 2.4)10^{-5}\mu M^2/s = (0.0007 - 0.0015)\mu M^2/min$. We then observe that D increases quite noticeably (from $\sim 0.0007\mu M^2/min$ to $\sim 0.5\mu M^2/min$) with the level of stimulation, *i.e.*, with β . If we restrict the calculation to either the medium or the low stimulation level experiments, however, D varies by at most a factor of 2. It is thus reasonable to consider a fixed D value in such a case. Now, for the Kramers calculation that yields Eq. (11) to hold it is necessary that $D \ll \Delta V_\beta$. This condition is not satisfied for most of the β values of Fig. 4 (c) if we use $D \sim (0.13 - 0.46)\mu M^2/min$, the estimate derived from the experiments with intermediate interspike times, while it is satisfied for $\beta \lesssim 0.18$ if we use the estimate obtained for long interspike times, $D \sim (0.0007 - 0.0015)\mu M^2/min$.

We show in Fig. 5 (b) the mean of the stochastic part of the interspike time, $\langle T_{IS} \rangle - T_{min}$, given by Eq. (11) as a function of $[IP_3]$ for $D = 0.0015\mu M^2/min$, where we have used Eq. (12) with $K_{IP} = 0.13\mu M$ to relate β and $[IP_3]$. The two straight lines drawn in the figure illustrate that $\langle T_{IS} \rangle - T_{min} \approx A \exp(-\lambda[IP_3])$ with $\lambda \approx 414/\mu M$ for the range, $0.172\mu M \lesssim [IP_3] \lesssim 0.179\mu M$ (for which $15min \lesssim \langle T_{IS} \rangle - T_{min} \lesssim 290min$) and with $\lambda \approx 195/\mu M$ for the range, $0.179\mu M \lesssim [IP_3] \lesssim 0.186\mu M$ (for which $4min \lesssim \langle T_{IS} \rangle - T_{min} \lesssim 15min$). We must recall that the curve in Fig. 5 (b) was obtained using a fixed value of D and the analysis of the previous paragraph showed that D increases significantly with the stimulation level, *i.e.*, with $[IP_3]$. Using two different values of D for the two $[IP_3]$ ranges covered by the straight lines in Fig. 5 (b) does not expand the exponential dependence over a larger region. Given the simplicity of the model considered here we can expect that the generic features of intracellular Ca^{2+} oscillations be reproduced but not necessarily (all) the quantitative aspects obtained in particular cell types. The impossibility of a quantitative agreement across cell types is immediately apparent in the significant differences among the values of T_{min} and $\langle T_{IS} \rangle$ obtained in each of the four combinations of cell type and effector probed and analyzed in [9]. But even if the individual T_{min} and $\langle T_{IS} \rangle$ values differ for the different experiments of [9], there are common features that the simple model is able to reproduce. For example, if we take an $[IP_3]$ interval over which the curve in Fig. 5 (b) is approximately an exponential function of $[IP_3]$ and compute the ratio between the values, $\langle T_{IS} \rangle - T_{min}$, obtained at the borders of this interval we can see that this ratio is larger than the equivalent one for most of the experiments reported in [9]. In particular, for the range $0.179\mu M \lesssim [IP_3] \lesssim 0.186\mu M$, this ratio is 3.75, which is about twice as large as the similar ratio for the experiments performed in rat primary hepatocytes in the presence of vasopressin (~ 2) and very close to the one obtained for human embryonic kidney (HEK293) cells in the presence of carbachol (~ 3.97) [9]. This means that the model is able to span a range of mean interspike periods which is similarly large to those observed in experiments in terms of the characteristic times of each cell type and effector probed. Perhaps the range of $[IP_3]$ values over which this behavior is encountered with the simple

model is relatively small compared with the real system (see discussion later). However, the ability to reproduce the range of mean interspike times is particularly relevant for the purpose that motivated the present work: unveiling the properties that characterize the encoding of external stimuli strengths in the frequency of pulsatile intermediaries of the signaling pathway.

In spite of the above discussion, we might still ask to what extent the derived exponential dependence of $\langle T_{IS} \rangle$ on $[IP_3]$ persists if the reduction to the fast manifold (Eq. (9)) and the theoretical expression, Eq. (11), are not used. To answer this question, we decided to perform stochastic simulations of Eqs. (3)–(4) with a noise term, ζ , added to Eq. (3) as previously done with Eq. (9). The rationale for adding a noise term solely to Eq. (3) is based on the assumption that Ca^{2+} puffs are the main source of fluctuations, an assumption we have already used to estimate the noise amplitude from experiments. Ca^{2+} puffs would add to the term proportional to v_{M3} in Eq. (3) which is not present in Eq. (4). On the other hand, other random events of Ca^{2+} entry from the extracellular medium (that would add to the terms proportional to v_0 or v_1 which are present in Eq. (4)) would be of smaller size and their effect would be negligible on Z (which is related to luminal $[Ca^{2+}]$ and typically much larger than C , see, *e.g.*, the discussion on the effect of Ca^{2+} puffs on luminal Ca^{2+} in [35]). We show in Fig. 6 (a),(b) two examples of C vs time obtained with the stochastic simulations performed using the *itoint* function of the *sdeint* package with $D = 0.0032\mu M^2/min$ and $\beta = 0.19$ ($[IP_3] = 0.176\mu M$) and $\beta = 0.18$ ($[IP_3] = 0.169\mu M$), respectively. We observe in both cases a sequence of randomly separated Ca^{2+} spikes (of $\sim 0.4min$ duration) where the mean interspike time is larger for the case with smaller β . We ran simulations of this type for a total simulation time of $10,000min$ and various values of β from which we computed the average interspike time, $\overline{T_{IS}}$, as a function of β . We show in Fig. 6 (c) the plot of $\overline{T_{IS}}$ as a function of $[IP_3]$ where the exponential dependence is apparent, as reflected by the red dashed straight line which corresponds to an expression of the form $\overline{T_{IS}} = 61min \exp(-329[IP_3]/\mu M)$. Given the typical values of $\overline{T_{IS}}$ and spike duration ($\sim 0.4min$), it is reasonable to assume that $\overline{T_{IS}} - T_{min} \approx \overline{T_{IS}}$, so that Figs. 6 (c) and 5 (b) are readily comparable, although it must be noticed that the former was obtained for a larger noise level because we were not restricted by the constraints of the theory. We observe that also in the case of Fig. 6 (c) a small change in $[IP_3]$ results in a relatively large range of $\overline{T_{IS}}$ values as obtained in Fig. 5 (b). The similarity is further reflected in the prefactor inside the exponential ($329/\mu M$ in Fig. 6 (c) vs $414/\mu M$ and $195/\mu M$ in Fig. 5 (b)).

In the experiments, the exponential dependence was found between the mean of the stochastic part of the interspike time and the external ligand concentration (vasopressin or carbachol in the two examples described in the previous paragraph). We should then ask whether the exponential dependence that we found between $\langle T_{IS} \rangle - T_{min}$ and $[IP_3]$ could also hold for the external stimulus strength, I_{ext} . As mentioned in the Introduction, IP_3 is produced as a result of the binding of external effectors to specific plasma membrane receptors. The external stimulus strength in our description

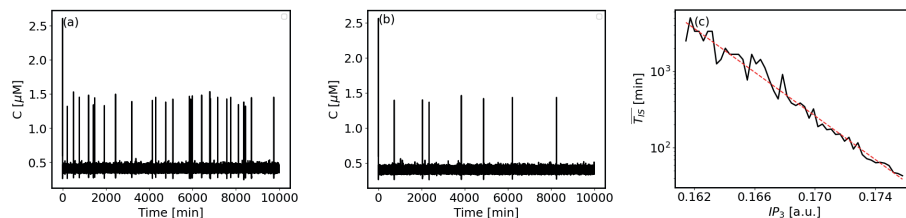


Figure 6. Results obtained with stochastic simulations of Eqs. (3)–(4) with the parameter values of Table 1, different values of β and a noise term, ζ , added to Eq. (3) as in Eq. (9), with $D = 0.0032\mu M^2/min$. Actually the corresponding Itô equations were solved using the *itoint* function of the *sdeint* package. (a), (b) Examples of C vs time obtained for $\beta = 0.19$ (i.e., $[IP_3] = 0.176\mu M$) and $\beta = 0.18$ (i.e., $[IP_3] = 0.169\mu M$), respectively. (c) Average interspike time, $\overline{T_{IS}}$, derived from one 10,000 min-long simulation for each β , as a function of $[IP_3]$ (solid line). The red dashed-line corresponds to an expression of the form $\overline{T_{IS}} = 61min \exp(-329[IP_3]/\mu M)$.

is thus proportional to the external effector concentration. The rate of IP_3 production is proportional to the mean number of effector-bound receptors which, in equilibrium, is typically a Hill function of the effector concentration. IP_3 , in turn, is degraded at a rate $\sim 0.11 - 0.14s^{-1}$ [40]. Thus, we can assume that, upon constant stimulation, $[IP_3]$ and I_{ext} are related by a nonlinear function of the form:

$$[IP_3] = [IP_3]_0 \frac{I_{ext}^h}{I_{ext}^h + K_D^h}, \quad (13)$$

where $h = 1$ for single site receptor binding of the extracellular effector as considered in [40]. Now, in our simple setting, the range of $[IP_3]$ over which the relation between $\langle T_{IS} \rangle - T_{min}$ and $[IP_3]$ is approximately exponential ($[0.172\mu M, 0.179\mu M]$ or $[0.179\mu M, 0.186\mu M]$ in Fig. 5 (b)) (and for which the range of mean interspike pulses is relatively wide compared with the experiments) entails at most a 4% variation in $[IP_3]$. Thus, a linearization of Eq. (13) would be relatively good in each of these ranges guaranteeing the exponential dependence between $\langle T_{IS} \rangle - T_{min}$ and I_{ext} as well. We could still wonder whether the function Eq. (13) is not saturated ($I_{ext} \gg K_D$). It is unlikely that the saturation of the IP_3 production be achieved for a situation with less than 20% of IP_3R occupation (represented by β in our model). On the other hand, $[IP_3]$ was estimated in *X. Laevis* oocytes to vary between $40nM$ at basal conditions and $\sim 1.8\mu M$ upon strong stimulation [41]. It is then reasonable to assume a linear relation between $[IP_3]$ and I_{ext} ($[IP_3] \approx [IP_3]_0 I_{ext}/K_D$ from Eq. (13) with $h = 1$) for situations, as those analyzed in this paper, in which $[IP_3] < 0.2\mu M$. We can still ask how realistic it is that a relative change in the mean interspike time as the one observed in the experiments be caused by a difference of a few nM in $[IP_3]$ as implied by Figs. 5 (b) and 6 (c). To answer this, we recall that the experiments performed in N1E-115 neuroblastoma cells under 30s stimulation with carbachol (CCh) [40] gave estimates of $[IP_3] \sim 10nM$ at basal levels and $[IP_3] \sim 35nM$ for $[CCh] = 1mM$. According to the analyses of [9], the mean interspike time obtained for HEK293 cells stimulated with

constant $CCh \in [30, 200] \mu M$ depended on $[CCh]$ as $\langle T_{IS} \rangle = T_{min} + B \exp(-\gamma[CCh])$ with $\gamma = 7.84/mM$. Assuming a linear relation between $[CCh]$ and $[IP_3]$, we can estimate $[IP_3] = 10nM + 25nM[CCh]/mM$ from the experiments of [40]. Assuming that a similar relation holds for the experiments performed in HEK293 cells stimulated with CCh [9] and using this expression to replace $[CCh]$ in terms of $[IP_3]$ in the function that relates $\langle T_{IS} \rangle$ and $[CCh]$ we obtain a $\sim 4.2nM$ difference between the extreme values of $[IP_3]$ probed in these experiments and $\langle T_{IS} \rangle = T_{min} + A \exp(-\lambda[IP_3])$ with $\lambda = \gamma mM/(25nM) = 313.6/\mu M$, remarkably similar to the values obtained with our very simple model ($414/\mu M$ and $195/\mu M$, for the two straight lines in Fig. 5 (b) and $329/\mu M$ for the one in Fig. 6 (c)). Based on this discussion we conclude that we have found a very plausible mechanistic explanation for the exponential dependence of $\langle T_{IS} \rangle - T_{min}$ with I_{ext} , as observed experimentally in [9].

6. Summary and conclusions

Cells use different strategies to decode the information they receive from the environment [2, 3, 4]. Very often, stationary external stimuli induce oscillations in some intermediaries of the signaling pathway with increasing frequencies as the stimulus strength grows [6, 7]. This *frequency encoding* strategy is very common when one of the intermediaries is intracellular Ca^{2+} , an ubiquitous signaling messenger that is involved in many different physiological processes [8, 11]. Although spatial non-uniformities play an important role on the dynamics of intracellular Ca^{2+} , many observations are reported in terms of spatial averages of the Ca^{2+} distribution. In this paper we focused on this type of observations, more specifically, on the sequences of Ca^{2+} pulses that have been observed in a variety of cell types in which Ca^{2+} is released from the Endoplasmic Reticulum (ER) through IP_3 receptors (IP_3Rs) upon constant stimulation [42]. The interpulse times have been found to have a relatively large stochastic component with an average that scaled exponentially with the extracellular stimulus strength [9]. Assuming that this behavior could be related to the excitability of the intracellular Ca^{2+} dynamics, in this paper we used a simple model in terms of ODEs with noise to derive theoretically and numerically this exponential scaling.

In this work we used the simple model of IP_3R -mediated intracellular Ca^{2+} dynamics of [33] for values of the fraction of IP_3 -bound IP_3Rs ready to become open upon Ca^{2+} binding, β , such that the system had only one stable and excitable stationary solution. Relying on the time scale separation of the processes, we restricted the dynamics to the fast manifold and analyzed the probability per unit time that noisy perturbations could elicit a long excursion in phase space (*i.e.* a spike). Assuming that the noisy perturbations were due to random localized events of Ca^{2+} entry into the cytosol which could be embraced in a single additive term, we used Kramers law to derive the said probability and the mean of the stochastic part of the interspike time, $\langle T_{stoch} \rangle \equiv \langle T_{IS} \rangle - T_{min}$. In this way we obtained an exponential dependence between $\langle T_{stoch} \rangle$ and the height of the (potential) barrier that the system had to cross to produce

a spike, ΔV_β , which, in turn, was a decreasing function of β (Fig. 4 (c)). Using the DeYoung-Keizer IP_3R model [34] to relate β and $[\text{IP}_3]$ (Eq. (12)) and estimating the noise level from experimental observations [16], we determined the relation between $\langle T_{stoch} \rangle$ and $[\text{IP}_3]$ (Fig. 5 (b)). In particular, we found that this relation could be approximated by an exponential over different $[\text{IP}_3]$ ranges (see the two straight lines in Fig. 5 (b)) that produced relatively wide $\langle T_{stoch} \rangle$ intervals (of the order of or larger than those observed experimentally [9]). Based on previous studies on the amount of IP_3 produced upon external stimulation in different cell types [40, 41] we could argue that $[\text{IP}_3]$ was linearly proportional to the external stimulus strength, I_{ext} , finding in this way a mechanistic explanation for the exponential dependence of $\langle T_{IS} \rangle - T_{min}$ with I_{ext} , observed in experiments [9].

The mechanistic explanation was initially derived restricting the dynamics of the model system to its fast manifold (Eq. (8)) and computing the mean interspike time using Kramers theory (Eq. (11)), which is valid in the low noise limit. This strategy has been used to analyze the dynamics of excitable systems when noise is added to the fast variable equation in the context of Self-Induced Stochastic Resonance (SISR) [24, 25]. Differently from the present paper where the interest lies on a regime where the sequence of spikes has a large stochastic component, these previous studies focused on the emergence of (quasi-regular) limit cycles due to noise. To the best of our knowledge, previous works have not looked at the aspect which motivated the present study: the exponential dependence between interspike time and stimulus strength, particularly, within the framework of cell signaling. We focused on this aspect because it endows cells with information transmission capabilities that are qualitatively different from other commonly used strategies of stimuli encoding [21]. We also studied to what extent the exponential dependence of $\langle T_{IS} \rangle$ on I_{ext} or equivalently, on β or $[\text{IP}_3]$, persisted if the reduction to the fast manifold and Kramers theory were not used. To this end, we performed stochastic simulations of Eqs. (3)–(4) with a noise term, ζ , added to Eq. (3). For the simulations we used a slightly larger noise amplitude since we were not restricted by the conditions of the theoretical derivation and obtained an exponential dependence that seemed to hold for larger $[\text{IP}_3]$ ranges than those obtained with the analytic derivation (Fig. 6). The results obtained with the same noise level as in Fig. 5 (b) were quantitatively similar to those of Fig. 5 (b) (data not shown). All these figures illustrate that the mechanism which underlies the occurrence of spikes in our model is such that a relatively large range of mean interspike times is spanned. As noted in [36], this is particularly advantageous for frequency encoding, but while in [36] it was argued that this situation could be achieved as a bifurcation was approached at which the period diverged, in our case this behavior derives from the escape rate from an excitable fixed point due to noise.

In this paper we used a model of the intracellular Ca^{2+} dynamics in terms of ODEs with noise in which the effect of the spatial inhomogeneities that are inherent to these signals were implicitly included in the noise term. Namely, as discussed in the previous Section, we used experimental results on the spatial inhomogeneities underlying

Ca^{2+} pulses to estimate the noise weight. There is always the possibility of using more realistic spatio-temporal models. In this regard, there are multiple options: intracellular Ca^{2+} signals involve processes that occur over many different length and time scales and models can describe each of these scales with more or less detail [43, 44, 45, 46, 47, 17, 48]. The choice of model depends on the type of question that the research seeks to answer and more detailed ones give more thorough mechanistic descriptions of the underlying processes [49, 50]. The simple model used here, however, provided an easily interpretable explanation of the exponential dependence between the stimulus strength and the mean interpulse time which can readily be applied to other pulsatile signaling agents.

A similar approach to the one described here can be applied in many other situations given the widespread presence of excitable dynamics in biology. Candidates to be described with this approach include Transcription Factors (TFs) that display bursts of nuclear translocation, for which there are several signs of noise induced processes. Examples of this behavior occur in the response to stress in yeast mediated by the TF, Msn2 [51], the differentiation in bacteria that could be described correctly with a noise-triggered excitable system [52] or the (mammalian) tumor suppressor, p53 [53], which dynamics requires an underlying excitable network structure [54]. It is relevant here to determine whether the pulses of nuclear localization or of activation of the intermediary of the transduction from the external stimulus to the response scale exponentially with the stimulus strength. We have found that this exponential dependence can endow frequency encoding with the ability to discriminate stimulus strengths equally well over a relatively wide range of intensities, making it qualitatively different from amplitude encoding [21]. Having a theoretical framework to account for this dependence gives support to the assumption that this qualitative difference occurs in many different settings. This idea is supported by the fact that the mean frequency of nuclear localization bursts of the TF, Crz1, in yeast can be shown to increase exponentially with extracellular Ca^{2+} [6] while the frequency of other TFs are convex increasing functions of the stimulus strength [55, 56] which, upon further scrutiny, might end up being exponential functions.

6.1. Acknowledgments

This research has been supported by UBA (UBACYT 20020170100482BA and 20020220300192BA) and ANPCyT (PICT 2018-02026 and PICT-2021-III-A-00091). SPD thanks the organizers of StatPhys28 for their support and cooperation.

6.1.1. References.

- [1] Gašper Tkačik and William Bialek. Information processing in living systems. *Annual Review of Condensed Matter Physics*, 7(1):89–117, 2016.
- [2] Filipe Tostevin, Wiet de Ronde, and Pieter Rein ten Wolde. Reliability of frequency and amplitude decoding in gene regulation. *Phys. Rev. Lett.*, 108:108104, Mar 2012.
- [3] Gabriele Micali, Gerardo Aquino, David M. Richards, and Robert G. Endres. Accurate encoding and decoding by single cells: Amplitude versus frequency modulation. *PLOS Computational Biology*, 11(6):1–21, 06 2015.

- [4] Alan Givré, Alejandro Colman-Lerner, and Silvina Ponce Dawson. Modulation of transcription factor dynamics allows versatile information transmission. *Scientific Reports*, 13(1):2652, 2023.
- [5] Richard C Yu, C Gustavo Pesce, Alejandro Colman-Lerner, Larry Lok, David Pincus, Eduard Serra, Mark Holl, Benjamin, Kirsten AU-Gordon, Andrew, and Roger Brent. Negative feedback that improves information transmission in yeast signalling. *Nature*, 456(7223):755–761, December 2008.
- [6] Long Cai, Chiraj K. Dalal, and Michael B. Elowitz. Frequency-modulated nuclear localization bursts coordinate gene regulation. *Nature*, 455(7212):485–490, Sep 2008.
- [7] Natalia Carbó, Nahuel Tarkowski, Emiliano Perez Ipiña, Silvina Ponce Dawson, and Pablo S. Aguilar. Sexual pheromone modulates the frequency of cytosolic ca^{2+} bursts in *saccharomyces cerevisiae*. *Molecular Biology of the Cell*, 28(4):501–510, 2017.
- [8] Genevieve Dupont, Laurent Combettes, Gary S. Bird, and James W. Putney. Calcium oscillations. *Cold Spring Harbor Perspectives in Biology*, 3(3), 2011.
- [9] Kevin Thurley, Stephen C Tovey, Gregor Moenke, Victoria L Prince, Abha Meena, Andrew P Thomas, Alexander Skupin, Colin W Taylor, and Martin Falcke. Reliable encoding of stimulus intensities within random sequences of intracellular ca^{2+} spikes. *Sci Signal*, 7(331):ra59, June 2014.
- [10] J. Kevin Foskett, Carl White, King-Ho Cheung, and Don-On Daniel Mak. Inositol trisphosphate receptor ca^{2+} release channels. *Physiological Reviews*, 87(2):593–658, 2007.
- [11] Martin D. Bootman. Calcium signaling. *Cold Spring Harbor Perspectives in Biology*, 4(7), 2012.
- [12] A Fabiato. Calcium-induced release of calcium from the cardiac sarcoplasmic reticulum. *Am J Physiol*, 245(1):1–15, 1983.
- [13] Y Yao, J Choi, and I Parker. Quantal puffs of intracellular ca^{2+} evoked by inositol trisphosphate in *xenopus* oocytes. *J Physiol (Lond)*, 482(3):533–553, 1995.
- [14] Xiao-Ping Sun, Callamaras Nicholas, Jonathan S Marchant, and Ian Parker. A continuum of InsP3-mediated elementary Ca^{2+} signalling events in *Xenopus* oocyte. *The Journal of Physiology*, 509(1):67–80, 1998.
- [15] Ian F. Smith and Ian Parker. Imaging the quantal substructure of single $ip3r$ channel activity during ca^{2+} puffs in intact mammalian cells. *Proceedings of the National Academy of Sciences*, 106(15):6404–6409, 2009.
- [16] Jonathan S. Marchant and Ian Parker. Role of elementary ca^{2+} puffs in generating repetitive ca^{2+} oscillations. *The EMBO Journal*, 20(1-2):65–76, 2001.
- [17] Lucia Lopez, Estefania Piegari, Lorena Sigaut, and Silvina Ponce Dawson. Intracellular calcium signals display an avalanche-like behavior over multiple lengthscales. *Frontiers in Physiology*, 3(350), 2012.
- [18] Lluís Hernández-Navarro, Sergio Faci-Lázaro, Javier G. Orlandi, Ulrike Feudel, Jesús Gómez-Gardeñes, and Jordi Soriano. Noise-driven amplification mechanisms governing the emergence of coherent extreme events in excitable systems. *Phys. Rev. Res.*, 3:023133, May 2021.
- [19] Eugene M. Izhikevich. *Dynamical Systems in Neuroscience: The Geometry of Excitability and Bursting*. MIT Press, Cambridge, MA, 2007.
- [20] Alan Givré and Silvina Ponce Dawson. Information content in stochastic pulse sequences of intracellular messengers. *Frontiers in Physics*, 6, 2018.
- [21] Alan Givré, Alejandro Colman-Lerner, and Silvina Ponce Dawson. Amplitude and frequency encodings give cells a different lens to sense the environment. to be published, 2023.
- [22] Peter Hänggi, Peter Talkner, and Michal Borkovec. Reaction-rate theory: fifty years after kramers. *Rev. Mod. Phys.*, 62:251–341, Apr 1990.
- [23] B. Lindner, J. Garcia-Ojalvo, A. Neiman, and L. Schimansky-Geier. Effects of noise in excitable systems. *Physics Reports*, 392(6):321 – 424, 2004.
- [24] Cyrill B. Muratov, Eric Vanden-Eijnden, and Weinan E. Self-induced stochastic resonance in excitable systems. *Physica D: Nonlinear Phenomena*, 210(3):227–240, 2005.
- [25] R. E. Lee DeVille, Eric Vanden-Eijnden, and Cyrill B. Muratov. Two distinct mechanisms of

- coherence in randomly perturbed dynamical systems. *Phys. Rev. E*, 72:031105, Sep 2005.
- [26] M C Eguia and G B Mindlin. Distribution of interspike times in noise-driven excitable systems. *Phys Rev E Stat Phys Plasmas Fluids Relat Interdiscip Topics*, 61(6 Pt A):6490–6499, June 2000.
- [27] James Lechleiter, Steven Girard, Ernest Peralta, and David Clapham. Spiral calcium wave propagation and annihilation in *xenopus laevis* oocytes. *Science*, 252(5002):123–126, 1991.
- [28] James D. Lechleiter and David E. Clapham. Molecular mechanisms of intracellular calcium excitability in *x. laevis* oocytes. *Cell*, 69(2):283–294, 1992.
- [29] Yue-Xian Li and John Rinzel. Equations for insp3 receptor-mediated $[ca^{2+}]_i$ oscillations derived from a detailed kinetic model: A hodgkin-huxley like formalism. *Journal of Theoretical Biology*, 166(4):461–473, 1994.
- [30] Y Tang and H G Othmer. Frequency encoding in excitable systems with applications to calcium oscillations. *Proceedings of the National Academy of Sciences*, 92(17):7869–7873, 1995.
- [31] Lukas Ramlow, Martin Falcke, and Benjamin Lindner. An integrate-and-fire approach to ca^{2+} signaling. part i: Renewal model. *Biophysical Journal*, 122(4):713–736, 2023.
- [32] Lukas Ramlow, Martin Falcke, and Benjamin Lindner. An integrate-and-fire approach to ca^{2+} signaling. part ii: Cumulative refractoriness. *Biophysical Journal*, 2023.
- [33] G Dupont and A Goldbeter. One-pool model for ca^{2+} oscillations involving ca^{2+} and inositol 1,4,5-trisphosphate as co-agonists for ca^{2+} release. *Cell Calcium*, 14(4):311–322, April 1993.
- [34] G W De Young and J Keizer. A single-pool inositol 1,4,5-trisphosphate-receptor-based model for agonist-stimulated oscillations in ca^{2+} concentration. *Proceedings of the National Academy of Sciences*, 89(20):9895–9899, 1992.
- [35] Lucia F Lopez and Silvina Ponce Dawson. Luminal ca^{2+} dynamics during ip3r mediated signals. *Physical Biology*, 13(3):036006, may 2016.
- [36] Stefan Schuster, Marko Marhl, and Thomas Höfer. Modelling of simple and complex calcium oscillations. *European Journal of Biochemistry*, 269(5):1333–1355, 2002.
- [37] Estefania Piegari, Lucia Lopez, Emiliano Perez Ipiña, and Silvina Ponce Dawson. Fluorescence fluctuations and equivalence classes of ca^{2+} imaging experiments. *PLOS ONE*, 9(4):1–18, 04 2014.
- [38] J Keener and J Sneyd. *Mathematical Physiology I: Cellular Physiology*. Springer, Berlin, 2009.
- [39] Luciana Bruno, Guillermo Solovey, Alejandra C. Ventura, Sheila Dargan, and Silvina Ponce Dawson. Quantifying calcium fluxes underlying calcium puffs in *xenopus laevis* oocytes. *Cell Calcium*, 47(3):273–286, 2010.
- [40] S S Wang, A A Alousi, and S H Thompson. The lifetime of inositol 1,4,5-trisphosphate in single cells. *Journal of General Physiology*, 105(1):149–171, 01 1995.
- [41] Veronica Luzzi, Christopher E. Sims, Joseph S. Soughayer, and Nancy L. Allbritton. The physiologic concentration of inositol 1,4,5-trisphosphate in the oocytes of *xenopus laevis* *. *Journal of Biological Chemistry*, 273(44):28657–28662, 1998.
- [42] Alexander Skupin, Helmut Kettenmann, Ulrike Winkler, Maria Wartenberg, Heinrich Sauer, Stephen C. Tovey, Colin W. Taylor, and Martin Falcke. How does intracellular ca^{2+} oscillate: By chance or by the clock? *Biophys. J.*, 94:2404–2411, 2008.
- [43] Silvina Ponce Dawson, Joel Keizer, and John E. Pearson. Fire–diffuse–fire model of dynamics of intracellular calcium waves. *Proceedings of the National Academy of Sciences*, 96(11):6060–6063, 1999.
- [44] Ana Calabrese, Daniel Fraiman, Daniel Zysman, and Silvina Ponce Dawson. Stochastic fire–diffuse–fire model with realistic cluster dynamics. *Phys. Rev. E*, 82:031910, Sep 2010.
- [45] Alejandra C. Ventura, Luciana Bruno, and Silvina Ponce Dawson. Simple data-driven models of intracellular calcium dynamics with predictive power. *Phys. Rev. E*, 74:011917, Jul 2006.
- [46] G. Solovey, D. Fraiman, B. Pando, and S. Ponce Dawson. Simplified model of cytosolic ca^{2+} dynamics in the presence of one or several clusters of ca^{2+} -release channels. *Phys. Rev. E*, 78:041915, Oct 2008.

- [47] Guillermo Solovey and Silvina Ponce Dawson. Intra-cluster percolation of calcium signals. *PLOS ONE*, 5(2):1–8, 02 2010.
- [48] V. Voorluijs, S. Ponce Dawson, Y. De Decker, and G. Dupont. Deterministic limit of intracellular calcium spikes. *Phys. Rev. Lett.*, 122:088101, Feb 2019.
- [49] Kevin Thurley and Martin Falcke. Derivation of ca^{2+}/sup_i signals from puff properties reveals that pathway function is robust against cell variability but sensitive for control. *Proceedings of the National Academy of Sciences*, 108(1):427–432, 2011.
- [50] Victor Nicolai Friedhoff, Benjamin Lindner, and Martin Falcke. Modeling ip3-induced ca^{2+} signaling based on its interspike interval statistics. *Biophysical Journal*, 122(13):2818–2831, 2023.
- [51] Natalia Petrenko, Razvan V Chereji, Megan N McClean, Alexandre V Morozov, and James R Broach. Noise and interlocking signaling pathways promote distinct transcription factor dynamics in response to different stresses. *Mol Biol Cell*, 24(12):2045–2057, April 2013.
- [52] Avigdor Eldar and Michael B. Elowitz. Functional roles for noise in genetic circuits. *Nature*, 467(7312):167–173, 09 2019.
- [53] Eric Batchelor, Caroline S. Mock, Irun Bhan, Alexander Loewer, and Galit Lahav. Recurrent initiation: A mechanism for triggering p53 pulses in response to dna damage. *Molecular Cell*, 30(3):277–289, 2008.
- [54] Gregor Mönke, Elena Cristiano, Ana Finzel, Dhana Friedrich, Hanspeter Herzog, Martin Falcke, and Alexander Loewer. Excitability in the p53 network mediates robust signaling with tunable activation thresholds in single cells. *Scientific Reports*, 7(1):46571, 2017.
- [55] Chiraj K. Dalal, Long Cai, Yihan Lin, Kasra Rahbar, and Michael B. Elowitz. Pulsatile dynamics in the yeast proteome. *Current Biology*, 24(18):2189–2194, 2014.
- [56] Nan Hao and Erin K O’Shea. Signal- dependent dynamics of transcription factor translocation controls gene expression. *Nature Structural & Molecular Biology*, 19(1):31–39, January 2012.